Copper Electrochemical Deposition Topography Regression

Hong Cai, and Xiaolin Xie

Abstract— **In this term project paper, new models to predict the pattern dependent topography after copper electroplating are developed by fitting the sequential data sets. The basic strategy is to choose the appropriate model items with the aids of CEAC model, a simple physical electroplating feature scale model. By screening the parameter candidates proposed by the physical model, regression of each experiment is carried. From the significance of each model parameter, we propose a new integrated model. The fitting goodness of the new models is compared with the previous model.**

Index Terms—**Regression, Response Surface Regression, Electroplating, Electrochemical Deposition (ECD), Chemical-Mechanical Polishing or Planarization (CMP), Topography, JMP.**

I. INTRODUCTION

Copper interconnect fabrication is an active and critical area of research and development in industry and academia to meet performance requirements for future advanced interconnect technologies with sub-micron dimensions. However, there are some fabrication problems in realizing the high yield and economic copper wiring in key process steps including copper deposition, patterning and planarization. Tradition aluminum interconnect fabrication technology cannot be transplanted to copper directly. In order to solve the fabrication problems, several new technologies are developed and introduced. Now dual damascene with chemical-mechanical polishing or planarization (CMP) and electrochemical deposition (ECD) is the predominant fabrication techniques for copper.

CMP provides local and global planarization ability to substitute for dry etching of copper, which suffers from the limited volatile copper compounds. ECD is very efficient to fill the damascene structure without voids and seams. The superconformal filling or superfilling ability is hard to be achieved by other copper deposition methods, like PVD.

Hong Cai is with the Microsystems Technology Lab, Massachusetts Institute of Technology, Cambridge, MA 02139 USA

Xiaolin Xie is with the Microsystems Technology Lab, Massachusetts Institute of Technology, Cambridge, MA 02139 USA

However, copper CMP suffers from problems of dishing and erosion, which are heavily dependent on underlying layout patterns such as pattern density or pattern pitch. The copper electroplated profile also suffers from pattern dependence. The initial non-uniform topography has a directly impact on the CMP polishing behavior and can further affect the non-uniformity problem in CMP. The polishing non-uniformity primarily results from the dishing and erosion, which is shown in Fig. 1, leads to considerable surface topography contributing to potential yield, reliability and manufacturability problems as well as process integration difficulties with other processes such as lithography.
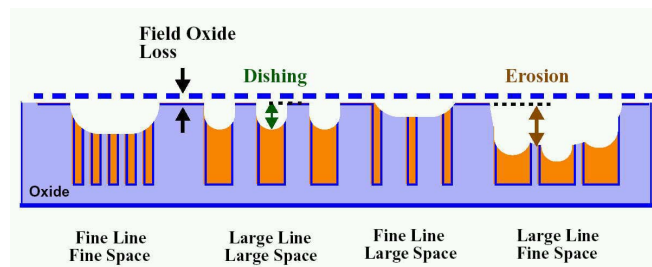

Fig. 1. Pattern Dependent Problems of Dishing and Erosion in Copper CMP [1].

In order to model the pattern dependence in copper interconnect fabrication processes, the as-deposited topography is required as an input of the CMP modeling. In this paper, we will discuss the ECD topography regression by implementing the data from a cooperation project with an outside company.

Experiments are performed using MIT/SEMATECH 854 multilevel test mask, which has copper line arrays of feature sizes in the range of 0.18 μm to 100 μm and layout densities in the range of 1% to 99% [1]. This test mask set has the ability to characterize the coupled pattern dependencies in copper electroplating and CMP processes. The mask and test structure layout are shown in Fig. 2.

Line width and line space are the key factors to affect the electroplated topography, which is characterized by two quantities (Step Height and Array Height), as shown in Fig. 3. Step height is defined as the bottom depth of each line with respect to the nearby surface, and the array height is defined as the top surface height of copper over an array region with respect to the flat copper field region over a wide oxide area

[1]. Tae developed semi-empirically analytical functions of line width and line space to express the electroplated topography, in terms of step height and array height.
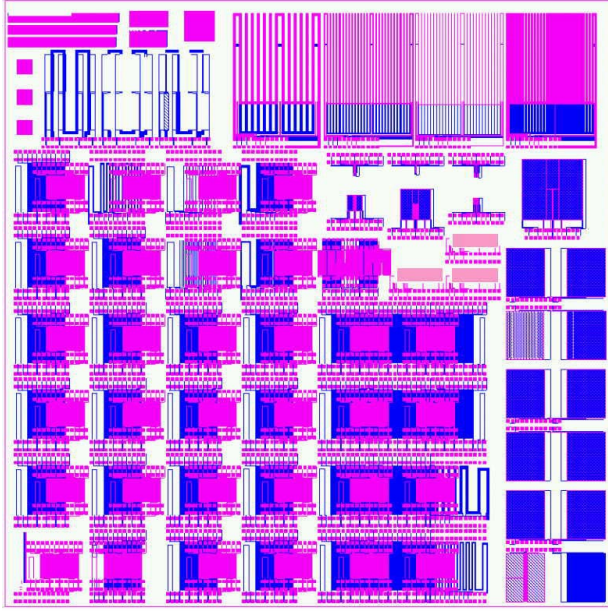

Fig. 2. Multilevel Test Mask Layout [1].
Metal 1: Blue (Dark); Metal 2: Magenta (Light).

The following content is organized into four sections. In Section 2, previous Park's regression models are review and implemented into the data for 5 splits with different copper thickness. Each split has two replicates. In Section 3, the optimum regression models for each step height and array height are searched from the candidate parameters derived from a physical electrochemical deposition model. Then, integrated models for *SH* and *AH* are presented in Section 4. The relations between the coefficients and the deposited copper thickness are briefly discussed. Finally, the new models are compared to Tae's models and a brief discussion is provided in Section 5.
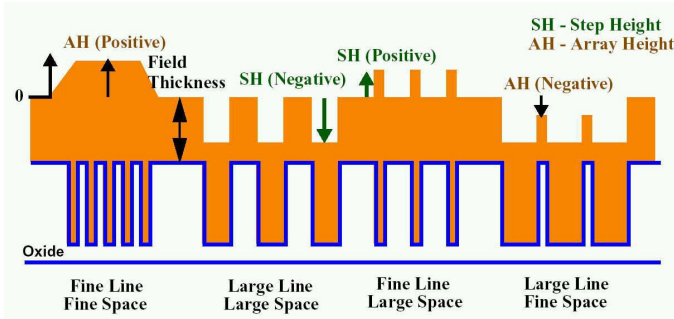

Fig. 3. Topography in Superfilling Copper Electroplating [1].

II.   PREVIOUS MODELS

A.   Review

To characterize as-deposited copper topography variation, a wafer is patterned with MIT 845 test mask and electroplated. Step height and array height are measured across many test pattern arrays and isolated features using a surface profiler. The absolute copper thickness is measured for translating relative surface height measurements into absolute thickness. The measured data is modeled as an empirical function of specific layout features by considering key pattern dependencies. After the model parameters are extracted, the electroplating pattern dependent model is calibrated and is ready to be used to perform chip-scale simulations for the electroplated surface topography for other chips fabricated using the calibrated electroplating process. The simulation result can be used as the initial input to MIT's CMP model.

Tae's electroplating pattern dependency model is based on a response surface regression [1]. This approach enables us to achieve the goal of chip-scale simulation, especially in dealing with random layouts. The following response models are used to capture step height and array height variations:

$$SH = A*lw + B*lw^{-1} + C*lw^2 + D*ls + E*lw*ls + Const. \quad (1)$$

$$AH = Ae*lw + Be*lw^{-1} + Ce*lw^{-2} + De*ls + Ee*lw*ls + Conste. \quad (2)$$

where *SH* is step height and *AH* is array height as defined Fig. 3. *lw* and *ls* are line width and line space, respectively, and *A*, *B*, *C*, *D*, *E*, *Const*, *Ae*, *Be*, *Ce*, *De*, *Ee*, and *Conste* are model coefficients. The interaction effect of *lw* and *ls* is reflected in the *lw*ls* non-additive item.

Park assigns any line widths greater than 10μm as 10μm and any line spaces greater than 10μm as 10μm. His argument is that if the line width is greater than the critical line width 10μm or the line space is greater than critical space 10μm, the *SH* and *AH* behavior remains almost constant, as shown in Fig. 4 and Fig. 5. Another reason is that some extraordinary line width and line space data make regression difficult. The new data set shows the same pattern, so the same line width and line space transformation is applied in the new model regression.
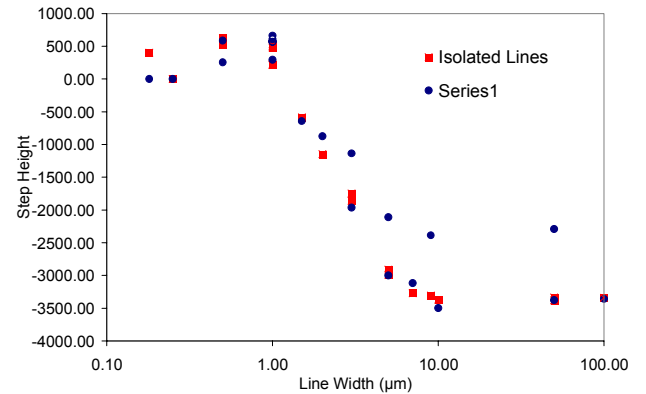

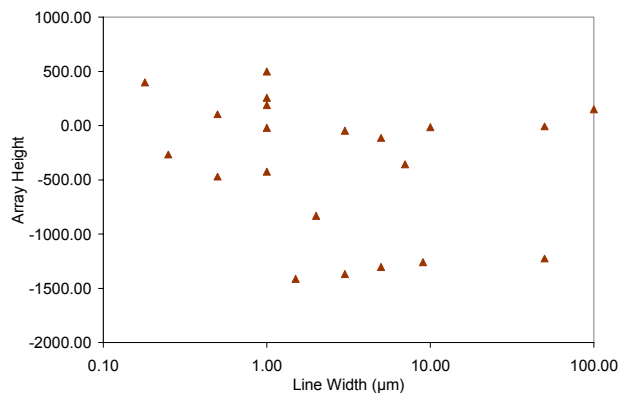Fig. 4. Step Height vs. Line Width for CPT104-slot1.

Fig. 5. Array Height vs. Line Width for CPT104-slot1.

B. Process Conditions

These wafer stack information for the wafers is Wafer film stack Si/AP-CVD TEOS 5000Å/AP-CVD PE-SiN 500 Å /AP-CVD 3000 Å /PVD Ta 300 Å /Cu seed 1500 Å /Cu EP. The electroplated copper thickness data are shown in Table 1. The trench depth is 3500 Å.

TABLE I
COPPER FILM THICKNESS

Wafer Number	Copper Thickness (Å)	Seed Layer Thickness (Å)	EP Copper Thickness (Å)
I: CPT115-slot1, 2	2664	1500	1164
II: CPT104-slot1, 2	8601	1500	7101
III: CPT115-slot4, 5	10350	1500	8850
VI: CPT105-slot1, 2	11696	1500	10196
V: CPT115-slot7, 8	14563	1500	13063

C. Model Implementation

JMP 4.1 is used to implement the previous models to fit the step height and array height for the new data sets. The results are summarized in Table II and Table III.

TABLE II
STEP HEIGHT REGRESSION RESULTS

Split		I	II	III	VI	V
R^2		0.965	0.973	0.968	0.970	0.949
R^2_{adj}		0.963	0.971	0.965	0.968	0.945
Lack of fit		32.295	10.738	10.661	7.687	18.437
CONST.	Est.	599.664	1602.657	1179.359	1510.908	746.353
	t	4.62	11.87	9.66	11.21	5.42
	Prob>$|t|$	<.0001	<.0001	<.0001	<.0001	<.0001
lw	Est.	-1140.785	-1235.590	-798.109	-965.676	-501.056
	t	-22.48	-23.43	-16.74	-18.34	-9.32
	Prob>$|t|$	<.0001	<.0001	<.0001	<.0001	<.0001
lw^{-1}	Est.	-52.793	-268.138	-228.850	-268.953	-163.640
	t	-1.63	-7.98	-7.54	-8.02	-4.78
	Prob>$|t|$	0.1064	<.0001	<.0001	<.0001	<.0001
lw^2	Est.	83.758	88.120	55.024	65.808	32.216
	t	19.02	19.26	13.30	14.40	6.91
	Prob>$|t|$	<.0001	<.0001	<.0001	<.0001	<.0001
ls	Est.	-5.629	25.789	29.894	14.622	43.711
	t	-0.56	2.47	3.16	1.40	4.10
	Prob>$|t|$	0.5773	0.0158	0.0022	0.1651	<.0001
$lw*ls$	Est.	-6.568	-16.269	-18.927	-18.662	-20.698
	t	-3.17	-7.55	-9.71	-8.67	-9.42
	Prob>$|t|$	0.0022	<.0001	<.0001	<.0001	<.0001

TABLE III
ARRAY HEIGHT REGRESSION RESULTS

Split		I	II	III	VI	V
R^2		0.685	0.796	0.881	0.861	0.908
R^2_{adj}		0.642	0.768	0.865	0.841	0.896
Lack of fit		5.081	20.801	24.873	12.658	12.105
CONST.	Est.	-435.685	-1283.287	-1579.862	-1626.250	-1455.446
	t	-3.13	-5.68	-7.82	-6.88	-7.71
	Prob>$|t|$	0.0035	<.0001	<.0001	<.0001	<.0001
lw	Est.	-10.027	-8.099	-29.371	-32.084	-78.773
	t	-0.51	-0.25	-1.03	-0.96	-2.95
	Prob>$|t|$	0.4486	0.0152	0.0004	0.0004	0.0002
lw^{-1}	Est.	-88.919	479.959	659.297	772.792	660.584
	t	-0.77	2.55	3.92	3.93	4.20
	Prob>$|t|$	0.4486	0.0152	0.0004	0.0004	0.0002
lw^{-2}	Est.	23.907	-37.132	-57.459	-76.130	-63.347
	t	1.25	-1.20	-2.08	-2.35	-2.45
	Prob>$|t|$	0.2182	0.2380	0.0450	0.0242	0.0193
ls	Est.	82.087	154.354	170.082	174.375	154.276
	t	5.92	6.87	8.46	7.42	8.21
	Prob>$|t|$	<.0001	<.0001	<.0001	<.0001	<.0001
$lw*ls$	Est.	-1.656	-1.325	0.188	1.430	4.401
	t	-0.78	-0.39	0.06	0.40	1.53
	Prob>$|t|$	0.4389	0.7017	0.9515	0.6926	0.1335

As we seen in the next two tables, the previous model woks well only for the step height regression. The lowest R^2 for the array height regression is up to 0.685.

III. INDIVIDUAL REGRESSION OPTIMIZATION

A. Physical Model Review

The previous models are not very good for the array height data sets. Furthermore it is hard to find physical meanings for the $lw*ls$ item. Improvement the model with more physical reasoning is needed. A simple ECD physical model is reviewed for the new model design.

Fig. 6. Filling contours predicted by the simple model (left) and the level-set code (right) [2]

In order to explain the superfilling behavior in electroplating with multi-component additives in the bath, Josell proposed a similar model named curvature enhanced accelerator coverage (CEAC) [2] to explain bump formation in a specific superfilling recipe. All adsorbed additives are assumed to keep on or float at the surface during deposition. The accumulation of adsorbed accelerator results from

reduction of surface area related to local surface curvature during growth. At the region of high positive curvature like the bottoms of small vias, increased local velocity is observed. A simple geometrical model can reduce the simulation time to less than one second by capturing the fundamentals of the near-optimized filling mechanics and using a first-order differential equation, as shown in Fig. 6.

Fig. 7. A Schematic of the Approximate Geometry for the Simple Model [2]

Straight vertical and horizontal lines simplify the time dependent interface shape in the trench, as shown Fig. 7. The local growth rate is experimentally derived and expressed in terms of the surface coverage of accelerator θ, overpotential η, the cupric ion concentration C at the interface and the bulk cupric concentration C_{cu} in the electrolyte:

$$\upsilon(\theta,\eta,C)=\frac{C}{C_{Cu}}\upsilon_o(\theta)\exp\left(-\frac{\alpha(\theta)F}{RT}\eta\right) \tag{3}$$

The evolution of accelerator coverage on the top, sidewalls and bottom of the trench is expressed in terms of the concentration of the accelerator $C_{Accelerator}$, the diffusion coefficient $D_{Accelerator}$, the number of available sites $\Gamma(1-\theta)$, a potential dependent rate constant $k(\eta)$, the sidewall growth rate υ_s and the bottom growth rate υ_b in (4), (5) and (6) .

$$\frac{d\theta_t}{dt}=\frac{C_{Accelerator}k(1-\theta_t)}{1+\delta\Gamma k(1-\theta_t)/D_{Accelerator}} \tag{4}$$

$$\frac{d\theta_s}{dt}=\frac{C_{Accelerator}k(1-\theta_s)}{1+\delta\Gamma k(1-\theta_s)/D_{Accelerator}} \tag{5}$$

$$\frac{d\theta_b}{dt}=\frac{C_{Accelerator}k(1-\theta_b)}{1+\delta\Gamma k(1-\theta_b)/D_{Accelerator}}+\frac{2\theta_s\upsilon_b}{w-2x}+\frac{2\theta_b\upsilon_s}{w-2x} \tag{6}$$

The horizontal displacements of the sidewalls and the vertical displacement of the bottom surface are expressed in (7) and (8).

$$x(t)=\int_0^t\upsilon[\theta_s(t),C_s(t)]dt=\int_0^t\upsilon_s(t)dt \tag{7}$$

$$y(t)=\int_0^t\upsilon[\theta_b(t),C_b(t)]dt=\int_0^t\upsilon_b(t)dt \tag{8}$$

Accounting for the effects of cupric ion depletion, the cupric ion concentration for the sidewalls C_s and the cupric ion concentration for the sidewalls C_s are written as (9) and (10) respectively.

$$C_s(t)=C_{Cu}-\frac{\delta\upsilon_s}{\Omega_{Cu}D_{Cu}} \tag{9}$$

$$C_b(t)=\left(1-\frac{(h+x-y)[2(h+x-y)\upsilon_s+(w-2x)\upsilon_b]}{(w-2x)(C_{Cu}\Omega_{Cu}D_{Cu}-\delta\upsilon)}\right)\times\left(C_{Cu}-\frac{\delta\upsilon}{\Omega_{Cu}D_{Cu}}\right) \tag{10}$$

All these equations describe the simplified trench filling process.

B. Individual Optimization Strategy

As we seen in the physical model review, the accumulation of adsorbed accelerator results from reduction of surface area related to local surface curvature during growth and the local growth velocity is a function of the accumulation of adsorbed accelerator. So the sidewall growth velocity, υ_s, and the bottom growth velocity, υ_b, will decide the as-deposited topography. So we can use lw^{-3}, lw^{-2}, lw^{-1}, *const* and even lw to express the local curvature. After integration, they are lw^{-2}, lw^{-1}, $ln(lw)$, lw and lw^2. That means that we can these items to express the as-deposited topography, or *SH* and *AH*. At the same time, we need to consider the cupric ion and additive concentration mass transportation and the effective cupric ion and additive concentration might depend on density *(lw/(lw+ls))*. As for the isolated lines, we assign 150 Å as the nominal line space only for density computation. Some non-addictive effects between *ls* and *lw* might be incorporated in to density denoted as *den*. IN park's models, *ls*lw* item is used to account for the non-addictive effects.

Therefore, we propose to choose lw^{-2}, lw^{-1}, $log(lw)$, lw, lw^2, ls^{-1}, $log(ls)$, ls, and *den* as regression model item candidates. The individual regression model optimization for each split will be implemented in the selected item range.

C. Optimization Implementation

TABLE VI
STEP HEIGHT REGRESSION RESULTS

Split		I	II	III	VI	V
R^2		0.973	0.953	0.928	0.941	0.890
R^2_{adj}		0.972	0.951	0.925	0.938	0.885
Lack of fit		23.082	19.553	25.480	16.788	40.480
CONST.	Est.	-88.117	1944.545	1577.098	1903.084	1181.318
	t	-1.22	11.7	9.29	10.76	6.27
	Prob>|t|	0.2247	<.0001	<.0001	<.0001	<.0001
lw^{-1}	Est.	-978.618	-281.505	-244.400	-284.286	-180.646
	t	-15.78	-6.42	-5.46	-6.1	-3.64
	Prob>|t|	<.0001	<.0001	<.0001	<.0001	0.0005
log(lw)	Est.	-6843.032				
	t	-22.16				
	Prob>|t|	<.0001				
lw	Est.	372.460	-1305.478	-879.414	-1045.843	-589.971
	t	12.57	-19.24	-12.68	-14.49	-7.67
	Prob>|t|	<.0001	<.0001	<.0001	<.0001	<.0001
lw^2	Est.		82.532	48.524	59.398	25.106
	t		13.98	8.05	9.46	3.75
	Prob>|t|		<.0001	<.0001	<.0001	0.0003
ls	Est.		-28.363	-33.104	-47.495	-25.184
	t		-2.86	-3.26	-4.49	-2.24
	Prob>|t|		0.0055	0.0016	<.0001	0.0281
den	Est.	371.976				
	t	4.01				
	Prob>|t|	0.0001				

The individual regression optimization results are list in

Table VI and Table V.

The R^2 for the array heights is improved dramatically. The results show that it is possible to build new integrated models to cover a broad rang of deposited copper thickness.

TABLE V
ARRAY HEIGHT REGRESSION RESULTS

Split		I	II	III	VI	V
R^2		0.892	0.937	0.949	0.923	0.970
R^2_{adj}		0.880	0.931	0.944	0.915	0.967
Lack of fit		0.539	4.788	8.954	5.763	2.554
CONST.	Est.	-717.607	117.668	-1230.939	-1171.685	-885.757
	t	-13.47	1.26	-15.17	-10.87	-9.47
	Prob>|t|	<.0001	0.2147	<.0001	<.0001	<.0001
lw^{-2}	Est.		-11.947			
	t		-2.83			
	Prob>|t|		0.0074			
lw^{-1}	Est.	64.596	277.803			426.910
	t	2.06	9.16			14.36
	Prob>|t|	0.0465	<.0001			<.0001
$log(lw)$	Est.			-1908.121	-2190.742	
	t			-9.53	-8.24	
	Prob>|t|			<.0001	<.0001	
lw	Est.		247.519	132.612	159.388	-331.084
	t		4.85	5.37	4.86	-8.45
	Prob>|t|		<.0001	<.0001	<.0001	<.0001
lw^2	Est.					24.909
	t					7.31
	Prob>|t|					<.0001
ls^{-1}	Est.	265.834		262.165	224.528	
	t	4.08		4.78	3.08	
	Prob>|t|	0.0002		<.0001	0.0039	
$log(ls)$	Est.	1693.294		1673.217	1709.023	1376.121
	t	7.46		16.22	12.47	25.58
	Prob>|t|	<.0001		<.0001	<.0001	<.0001
ls	Est.	-94.337				
	t	-4.54				
	Prob>|t|	<.0001				
den	Est.		-2754.783			
	t		-20.83			
	Prob>|t|		<.0001			

IV. INTEGRATED MODELS

Based on the results of individual regression optimization, the new integrated models are presented in the following two equations:

$$SH = A * lw^{-1} + B * lw + C * lw^2 + D * ls + Const. \qquad (11)$$

$$AH = Ae * lw^{-1} + Be * \log(lw) + Ce * lw + De * ls^{-1} + Ee * \log(ls) + Conste. \qquad (12)$$

where SH is step height and AH is array height, lw and ls are line width and line space, respectively, and A, B, C, D, $Const$, Ae, Be, Ce, De, Ee, and $Conste$ are model coefficients. Table VI and Table VII show the regression results of the new integrated models.

Compared to the previous models, the only difference for the step height regression is that there is no $lw*ls$ item. The exclusion of the non-physical item affects little in the fitting goodness except the last split. The results justify our strategy to introduce more physical meaning in the model design. On the other hand, the new models fit the array height much better

than the previous model. The lowest R^2 for the array height regression is equal to 0.864. The lack of fit in the array height is insignificant. What we need pay attention is that the t values are overestimated due to the under-estimation of the pure error. The calculated pure error is 100Å or so, however the raw data noise level is 200~300Å. The new items of $log(lw)$ and $log(lw)$ make the new model reflect more physical process in feature scale.

TABLE VI
STEP HEIGHT REGRESSION RESULTS

Split		I	II	III	VI	V
R^2		0.961	0.953	0.928	0.941	0.890
R^2_{adj}		0.959	0.951	0.925	0.938	0.885
Lack of fit		35.174	19.553	25.480	16.788	40.480
CONST.	Est.	737.683	1944.545	1577.098	1903.084	1181.318
	t	5.71	11.70	9.29	10.76	6.27
	Prob>|t|	<.0001	<.0001	<.0001	<.0001	<.0001
lw^{-1}	Est.	-58.189	-281.505	-244.400	-284.286	-180.646
	t	-1.71	-6.42	-5.46	-6.10	-3.64
	Prob>|t|	0.0916	<.0001	<.0001	<.0001	0.0005
lw	Est.	-1168.999	-1305.478	-879.414	-1045.843	-589.971
	t	-22.16	-19.24	-12.68	-14.49	-7.67
	Prob>|t|	<.0001	<.0001	<.0001	<.0001	<.0001
lw^2	Est.	81.502	82.532	48.524	59.398	25.106
	t	17.77	13.98	8.05	9.46	3.75
	Prob>|t|	<.0001	<.0001	<.0001	<.0001	0.0003
ls	Est.	-27.490	-28.363	-33.104	-47.495	-25.184
	t	-3.56	-2.86	-3.26	-4.49	-2.24
	Prob>|t|	0.0006	0.0055	0.0016	<.0001	0.0281

TABLE VII
ARRAY HEIGHT REGRESSION RESULTS

Split		I	II	III	VI	V
R^2		0.864	0.936	0.949	0.923	0.961
R^2_{adj}		0.845	0.927	0.942	0.912	0.956
Lack of fit		1.201	5.306	9.638	6.193	4.122
CONST.	Est.	-694.6	-1116.0	-1226.3	-1159.6	-1141.8
	t	-11.0	-12.9	-13.5	-9.6	-13.5
	Prob>|t|	<.0001	<.0001	<.0001	<.0001	<.0001
lw^{-1}	Est.	376.3	582.8	-17.2	-44.4	64.1
	t	3.9	4.3	-0.1	-0.2	0.5
	Prob>|t|	0.0005	0.0001	0.9032	0.8137	0.6277
$log(lw)$	Est.	789.5	-231.3	-1951.2	-2301.7	-2010.4
	t	2.8	-0.6	-4.8	-4.3	-5.3
	Prob>|t|	0.0081	0.5555	<.0001	0.0001	<.0001
lw	Est.	-58.5	33.2	135.6	167.1	125.6
	t	-2.4	1.0	3.9	3.6	3.9
	Prob>|t|	0.0210	0.3269	0.0004	0.0009	0.0004
ls^{-1}	Est.	-100.3	-215.9	273.5	253.6	142.4
	t	-1.3	-2.1	2.5	1.8	1.4
	Prob>|t|	0.1879	0.0432	0.0155	0.0845	0.1638
$log(ls)$	Est.	565.9	1031.7	1684.2	1737.2	1572.0
	t	5.9	7.8	12.2	9.5	12.3
	Prob>|t|	<.0001	<.0001	<.0001	<.0001	<.0001

We plot the residuals of array height fitting with Tae's model and our integrated model in Fig. 8 and Fig. 9. The residual of the integrated model is more uniformly packed around zero compared with that of Tae's model.

Generally, the coefficients are roughly consistent in the sign and magnitude except the first split with the thinnest electroplated copper film. There is no surprise for this extraordinary result. In fact the coefficients for the fist split

reflect the initial deposition stage. One reasonable derivation from the physical model is that the topography can be kept in some steady state or quasi-steady state after certain deposited film thickness due to the final additive concentration equilibrium. The direct results are the similar coefficients in the last four splits. Some variations in their coefficients can be explained by the data contamination due to the measurement tool limits.
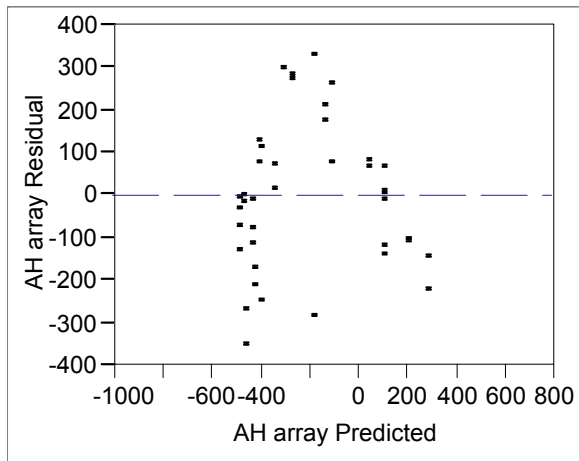

Fig. 8.   Residual plot for AH of CPT104 using Tae's model
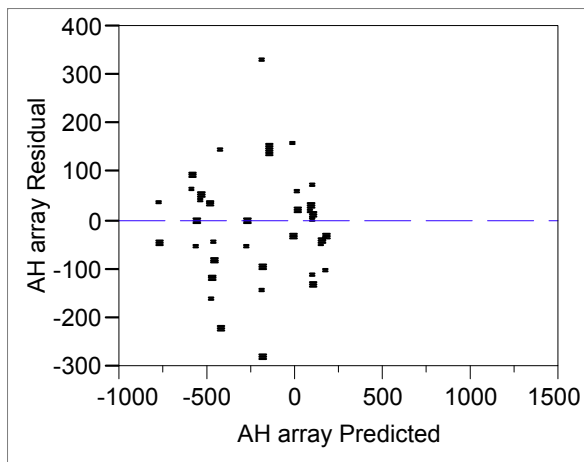
Fig. 9.   Residual plot for AH of CPT104 using the integrated model

V.   CONCLUSION

In this term project paper, new models to describe the pattern dependent topography after copper electroplating are developed for fitting the sequential data sets. The basic strategy is to choose the appropriate model items with the aids of a simple physical electroplating feature scale model. By screening the item candidates proposed by the physical model, individual regression optimization are carried. The results provide the guidance for the desired integrated models, which can cover a broad range of copper film thickness. The new models are helpful to implement the CMP modeling in the further research.

The fitting goodness of the new models is presented with the previous model results. The apparent improvement in physical basis brings the power to fix the defect in the array height modeling in the previous work.

Further research on the qualitative relation between the coefficients and the deposited film thickness is desired. It will give us more freedom to predict the topography without the tedious experiments and the ability to co-optimize the CMP and ECD processes and then decrease the environment load. However, more high-resolution data are necessary for such a task.

REFERENCES

[1]   T. Park, "Characterization and Modeling of Pattern dependencies in Copper Interconnects for Integrated Circuits," Ph.D. Thesis, Electrical Engineering and Computer Science, MIT, May 2002.
[2]   D. Josell, D. Wheeler, W. H. Huber, J. E. Bonevich, and T. P. Moffat, "A Simple Equation for Predicting Superconformal Electrodeposition in submicrometer Trenches", J. Electrochem. Society, Vol. 148, No. 12, pp. 767-773, 2001.

Hong Cai received the dual B.S. degrees in materials science & engineering and economics from Tsinghua University, Beijing, P.R.C., in 1998, and the M.S. degree in materials science & engineering from Tsinghua University. He is currently pursuing the Ph.D. degree in the Department of Materials Science and Engineering, MIT.
   From 1997 to 2000, he worked on composite multilayer ceramic capacitor. In the following two year, his research interest was non-lead ferroelectrics project supported by NSF and DARPA. Since 2002, he has been a member of Microsystems Technology Lab, MIT. His current research is focus on the multilevel metallization modeling and simulation and chemical- mechanical polishing (CMP) test mask design.

Xiaolin Xie received B.S. degree in physics from Caltech in 2000. He is currently pursuing the Ph.D. degree in the Physics Department, MIT.
   From 2000 to 2001, he studied transport property of artificial solid. He joined Microsystems Technology Lab at the beginning of 2002. His current research is focus on modeling of STI chemical mechanical polishing (CMP) modeling and nanotopography in CMP.